JASA EXPRESS LETTERS

Synthesis of wind turbine trailing edge noise in free field

Cite as: JASA Express Lett. **2**, 033601 (2022); https://doi.org/10.1121/10.0009658
Submitted: 23 December 2021 • Accepted: 09 February 2022 • Published Online: 03 March 2022

David Mascarenhas, Benjamin Cotté and Olivier Doaré

JASA EXPRESS LETTERS ARTICLE asa.scitation.org/journal/jel

Synthesis of wind turbine trailing edge noise in free field

David Mascarenhas, Benjamin Cotté, and Olivier Doaré[a)]
Institute of Mechanical Sciences and Industrial Applications, École Nationale Supérieure de Techniques Avancées Paris, Centre National de la Recherche Scientifique, Commissariat à l'Énergie Atomique et aux Énergies Alternatives, Électricité de France, Institut Polytechnique de Paris, Paris, France
david.mascarenhas@ensta-paris.fr, benjamin.cotte@ensta-paris.fr, olivier.doare@ensta-paris.fr

Abstract: The proposed sound synthesis tool converts a physics-based frequency-domain model of wind turbine trailing edge noise to a time-domain signal while accounting for the appropriate time shift due to the propagation between the moving blades and the fixed observer. A window function that implements cross-fading between consecutive signal grains is proposed and a method to objectively estimate the influence of the synthesis parameters is described. As the synthesis tool is independent of the aerodynamic noise model, it can be readily adapted to auralize other noise sources such as turbulent inflow noise or stall noise.

[Editor: Con Doolan] https://doi.org/10.1121/10.0009658

Received: 23 December 2021 **Accepted:** 9 February 2022 **Published Online:** 3 March 2022

1. Introduction

Noise from modern wind turbines is dominated by broadband aeroacoustic mechanisms generated by the interaction between turbulent flow fluctuations and the rotating blade edges. The amplitude modulation of this broadband noise is known to be a potential source of annoyance for people living in the vicinity of wind farms (Hansen *et al.*, 2021; Pedersen and Persson Waye, 2004). The main sources of broadband noise are turbulent inflow noise (TIN), trailing edge noise (TEN), and stall noise (Bertagnolio *et al.*, 2017; Oerlemans and Schepers, 2009). Among these noise sources, stall noise is the most intense but is produced only when the angle of attack is large, whereas TIN and TEN occur for all angles of attack. Thus, in the simplest case scenario it can be said that TIN and TEN are observed at all times for an operating wind turbine and are the dominant sources of wind turbine noise. The synthesis of these noise sources would be valuable to understand the auditory perception and psychoacoustics that relates to the annoyance caused by wind turbine noise. Auralization of different outdoor noise sources that have been studied extensively are either sample-based (Georgiou *et al.*, 2019; Jagla *et al.*, 2012) or physics-based (Arntzen and Simons, 2014; Pieren *et al.*, 2017). Sample-based auralization previously done for wind turbine noise covers a few prevailing parameters and can be difficult to extend further to compensate for other settings (Pieren *et al.*, 2014). This restriction occurs because the sample-based synthesis is directly dependent on the noise recordings which are known to be often contaminated with background noise and wind noise (Bolin *et al.*, 2010; Van den Berg, 2006). There is hence a need for a physics-based auralization, as it allows for a greater control over the desired physical parameters that contribute to the noise generating acoustics.

Various frequency-domain models of wind turbine noise sources have been proposed in the literature (Bertagnolio *et al.*, 2017; Oerlemans and Schepers, 2009; Tian and Cotté, 2016). To focus on the synthesis method only the TEN model described in Tian and Cotté (2016) is used here as the base physical model but the same synthesis method can be used with any frequency-domain TEN model and can also be extended to include TIN and stall noise. Note that Lee *et al.* (2013) propose a different synthesis method that models aerodynamic noise directly in the time domain based on the Ffocws Williams and Hawkings analogy.

The main objective of this article is to present a method which converts the frequency-domain model into a time-domain signal, while also accounting for appropriate physical parameters such as time delay due to propagation and geometrical spreading. The resulting synthesized signal is the TEN that is generated by the wind turbine blades in rotation, experienced by an observer in free field. The sound synthesized for an observer on the ground with this method is comparable to the wind turbine noise recorded at the IEC point (IEC, 2012). The described synthesis tool coupled with virtual reality or augmented reality can be useful to predict the noise generated by potential wind farms in the design phase. The paper first explains briefly the frequency-domain prediction model for the TEN as well as its important parameters in

[a)]ORCID: 0000-0003-2219-9295.

Sec. 2. The conversion of the frequency spectra to the time-domain signal is detailed in Sec. 3 followed by the description of how the propagation delay is accounted for. Some crucial parameters that are used for the synthesis are studied in detail in Sec. 4 and a few test cases of signals synthesized by this method are presented in Sec. 5.

2. Frequency-domain modelling of trailing edge noise for a wind turbine

The turbulent boundary layer fluctuations convected at the velocity U_c interact with the trailing edge of an airfoil to generate trailing edge noise. For a fixed airfoil of span L and chord c, the original model proposed by Amiet (1976) predicts the noise generated by the trailing edge of a fixed airfoil assimilated to a thin plate interacting with turbulent gusts of uniform velocity. The power spectral density (PSD) of the acoustic pressure due to the TEN produced by an airfoil of large aspect ratio ($L > 3c$) that is observed in the far field (x_R, y_R, z_R) is given by (Roger and Moreau, 2010)

$$S'_{pp}{}^{\mathrm{TEN}}(x_R, y_R, z_R, \omega) = \left(\frac{kcz_R}{4\pi S_0^2}\right)^2 2L\,\Phi_{pp}(\omega)\,l_y\left(\omega, \frac{ky_R}{S_0}\right)\left|\mathcal{L}_{TE}\left(x_R, \frac{\omega}{U_c}, \frac{ky_R}{S_0}\right)\right|^2, \tag{1}$$

where ω is the angular frequency, k is the acoustic wavenumber, S_0 is the modified distance between the source and the observer, Φ_{pp} is the wall pressure fluctuation spectrum, l_y is the spanwise correlation length estimated by the Corcos model, and $\mathcal{L}_{TE}$ is the transfer function for trailing edge noise. By dividing a wind turbine blade into segments with the appropriate aspect ratio and twist, Tian and Cotté (2016) extended this noise prediction model to a full size wind turbine. The wall pressure fluctuation spectrum Φ_{pp} used here is calculated using the model of Goody (2004) for the pressure side and the model of Rozenberg *et al.* (2012) for the suction side of the airfoil.

As a rotating blade experiences non-uniform flow along the span, with the incoming velocity strongest at the blade tip, the segmentation of the blade allows for the implementation of different inflow velocities for each segment. The segmentation is done ensuring the segment span is greater than the spanwise turbulence correlation length. The frequency-domain model approximates the complete rotation of the blade as a series of translations between discrete angular positions. The convective amplification and Doppler effect caused by the rotating blades is also accounted for following Sinayoko *et al.* (2013). The instantaneous PSD at the observer for an azimuthal blade position β is given by

$$S_{pp}(\mathbf{x_0}, \omega, \beta) = \left(\frac{\omega_e}{\omega}\right) S'_{pp}(\mathbf{x}, \omega_e, \beta), \tag{2}$$

where $S'_{pp}(\mathbf{x}, \omega_e, \beta)$ given by Eq. (1) is the PSD for a fixed blade, ω_e and ω are the emitted and observed frequencies, and $\mathbf{x_0}$ and $\mathbf{x}$ are the observer coordinates in the hub and blade coordinate systems. The implemented source model for a full size wind turbine thus gives the frequency-domain response of each segment of each blade at each discrete angular position β [Fig. 1(a)]. This response is obtained for an observer at a position defined by the angle τ with respect to the wind direction and by the horizontal distance R from the base of the wind turbine tower as shown in Fig. 1(a).

3. Sound synthesis method

As each of the segments of the wind turbine blades are assumed to be uncorrelated to each other and contribute individually to the total noise, they can be synthesized separately and then summed together at each time step. The contribution from one segment between two successive blade angular positions is referred to as a grain in this study. We first discuss

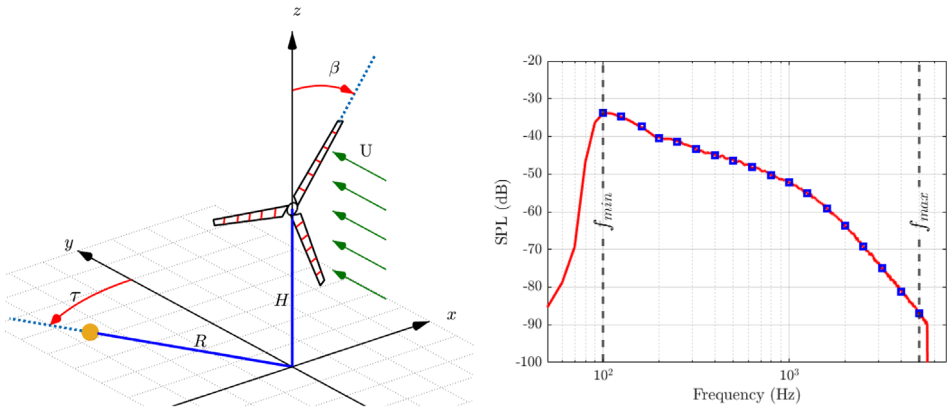

(a) (b)

Fig. 1. (a) Schematics for the wind turbine sound synthesis tool with the receiver represented as a sphere. (b) Plot of the desired input PSD (blue squares) compared to the PSD with 10 Hz resolution of the resulting grain (red).

in Sec. 3.1 an efficient method to synthesis a single grain, which converts the PSD to a time-domain signal of the correct length. The cross-fading window function used for the smoothing of the transitions between grains is discussed in Sec. 3.2.

3.1 Conversion from frequency-domain spectra to time-domain signal

The PSD of the acoustic pressure obtained from the frequency-domain model of the airfoil noise is calculated for a set of frequencies between f_{min} and f_{max}. The pressure amplitude corresponding to a particular frequency can be directly calculated as

$$p(f) = \sqrt{1\,\text{Hz} \cdot S_{pp}(f)}\,(\text{Pa}). \tag{3}$$

The spectrum obtained from this equation provides information over a finite number of frequency bins. As the inverse discrete Fourier transform (IDFT) converts a frequency-domain spectrum into a time-domain signal while conserving the same number of data points, the number of frequency bins may be insufficient to obtain a time signal of desired length with a typical sampling frequency of 44.1 kHz. To obtain the desired duration of the signal, the amplitude spectrum is interpolated within the frequency range $[f_{\text{min}}, f_{\text{max}}]$ of the input PSD, while the pressure amplitudes for the other frequencies outside the limits are taken as zero. The number of points of the one-sided spectrum corresponds to the total number of frequency bins that include the interpolated amplitude spectrum and the frequencies with zero amplitude. As the noise is assumed to be stochastic, a random phase between 0 and 2π is assigned to each of the complex amplitudes in this one-sided frequency spectrum. The one-sided frequency spectrum is converted to a symmetric double-sided frequency spectrum and the IDFT is taken, thus obtaining a real-valued time-signal.

The signal is synthesized for a larger time duration and then truncated as desired. This synthesized signal obtained from the PSD corresponding to one segment is the grain under consideration. A grain synthesized between $f_{min} = 100$ Hz and $f_{max} = 5000$ Hz with 18 frequency points that correspond to the center frequencies of the third octave bands shows a good replication of the desired input PSD as seen in Fig. 1(b).

The time duration of the emitted noise as observed by the receiver is the required grain size. This involves the emission time Δt_s between the angular step $\Delta\beta$ and the propagation time between the segment and the receiver. If the distance between the source and the receiver is $r(\beta)$, the time duration of the emitted noise as observed by the receiver is given by

$$T_{\Delta\beta} = \Delta t_s + \frac{\Delta r}{c_0} = \frac{\Delta\beta}{\Omega} + \frac{\Delta r}{c_0}, \tag{4}$$

where Ω is the rotational speed of the wind turbine blade and $\Delta r = r(\beta_n) - r(\beta_{n-1})$ is the difference between the propagation distances related to the corresponding successive angular positions that can be positive or negative. The grain of duration $T_{\Delta\beta}$ contains $N_{\Delta\beta}$ samples which depends on the sampling frequency.

3.2 Cross-fading window function

Audio reproduction of the successive grains produce artifacts in the form of clicks during the transition of grains that do not have continuity in amplitude. To avoid this form of artifact, the transition between grains has to be done with a certain amount of overlap between each grain, while still conserving the absolute size of each grain. Such transitions of audio signals are commonly known as cross-fading (Langford, 2013). To facilitate the cross-fading between two grains, a window function is designed and applied to each grain. The window function $W[k]$ of N samples is composed of the overlapping functions $f[k]$ and $g[k]$ with a unit response between them and can be defined as

$$W[k] = \begin{cases} f[k] & \text{for} \quad 1 \le k < w_l \\ 1 & \text{for} \quad w_l \le k \le N - w_l \\ g[k] & \text{for} \quad N - w_l + 1 < k \le N, \end{cases} \tag{5}$$

where w_l is the desired length of the overlap function that is to be set (Fig. 2). The overlapping functions $f[k]$ for the fade-in and $g[k]$ for the fade-out are required to serve the purpose of overlapping between two grains, such that the original power is conserved during the overlap. The synthesized signal is thus a linear combination of the two successive grains where the window functions can be seen as weights.

To avoid inconsistencies in the overlap amount it is necessary to keep constant the length of the overlapping function for all grains even though the size of each grain differs. This is done by setting a constant length w_l for the functions $f[k]$ and $g[k]$ for all the grains, while the variability of the grain length is achieved by adjusting the length of the unit response between the overlap functions: $N_{unit} = N - 2w_l$.

To be consistent with the length of the overlap functions and the size of the grains, the length w_l is divided equally between the two successive grains. As shown in Fig. 2(a), the overlapping length w_l can be written as a function of the length of the grain $N_{\Delta\beta}$ and the length of the unit response N_{unit},

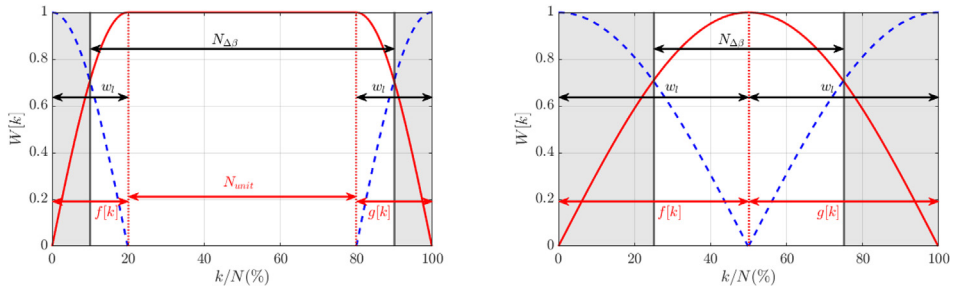

Fig. 2. The window function $W[k]$ of length $\mathrm{N} = N_{\Delta\beta} + w_l$ with the overlapping window functions $f[k]$ and $g[k]$ with (a) $\Psi = 40\%$ and (b) $\Psi = 100\%$ of overlap (red solid line). The white area indicates the grain in consideration and the gray shaded area indicates the previous and next grains. The blue dashed lines represent the overlap functions of the adjacent grains.

$$w_l = N_{\Delta\beta} - N_{unit}. \tag{6}$$

This gives us the maximum possible length for the overlap function w_l which corresponds to the smallest grain in the system and to $N_{unit} = 0$: $w_l = \min(N_{\Delta\beta})$. The length of the overlap function w_l is thus restricted to $0 \leq w_l \leq \min(N_{\Delta\beta})$. The amount of overlap is defined as

$$\Psi = \frac{w_l}{\min(N_{\Delta\beta})}, \tag{7}$$

with $0 \leq \Psi \leq 1$. The defined window function is plotted in Fig. 2 with $\Psi = 40\%$ and $\Psi = 100\%$ of overlap calculated for the smallest grain. It can be seen in Fig. 2(b) that N_{unit} is equal to zero for $\Psi = 100\%$. To adapt to a larger grain size, the length of the unit response is increased while the overlap amount w_l is kept the same.

The main purpose for the cross-fading window is to facilitate a smoother transition from one grain to the next while maintaining the proper power level. For two signals to cross-fade while preserving their respective power level during the transition, the cross-fade functions g and f must satisfy (Fink *et al.*, 2016)

$$f^2 + 2 \cdot f \cdot g \cdot r_{(p_1,p_2)} + g^2 = 1, \tag{8}$$

where $r_{(p_1,p_2)}$ is the correlation coefficient of the two overlapping signals p_1 and p_2, which is zero for uncorrelated signals and one for completely correlated signals. As we assume that successive grains are uncorrelated giving $r_{(p_1,p_2)} = 0$, Eq. (8) satisfies the Princen-Bradley criterion (Bäckström, 2019). Following Fink *et al.* (2016), a number of functions satisfying these conditions are available for the selection of the cross-fading overlap function. The simplest and efficient functions for the windows are given by $f(\chi) = \sin(\pi\chi/2)$ and $g(\chi) = \cos(\pi\chi/2)$, where $\chi \in [0, 1]$ is the normalized time index. These functions used in Eq. (5), with the desired length of the overlap function w_l determined by Eq. (7) define the window function that is used to facilitate the cross-fading between two successive grains.

4. Influence of the overlap amount in the cross-fading between grains and the number of angular position

In the synthesis model the overlap amount determined by Ψ and the number of discrete angular positions N_β influence the smoothness of the synthesized signal. To understand their individual contribution a single segment is synthesized. The trailing edge noise emitted by the tip segment of one wind turbine blade at a radial distance of 45 m, rotational speed $\Omega = 1.47$ rad/s and hub height of $H = 80$ m is synthesized for a receiver at the crosswind position ($\tau = 90°$) with the distance of $R = 100$ m from the base of the hub. This position is chosen as the amplitude modulation is maximum at the cross-wind. The wind inflow velocity is taken to be 8 m/s for all heights. The system is synthesized for different values of Ψ, between 1% and 100% and different values of N_β from 12 to 72 angular positions.

A moving RMS over 50 ms is used as an envelope function to detect the changes in the synthesized signal that relate to the contribution of individual grains. The time duration of the moving window is well adapted to detect the structural differences in the signal as the minimum grain duration in the system is larger than 50 ms. The change in the amplitude of the grains is quantified by taking the sound pressure level (SPL) of the time derivative of the moving RMS which is defined by

$$L_{dp}(t) = 10\,\log_{10}\left(\frac{(dp_{\mathrm{rms,50ms}}(t)/dt)^2}{(p_{\mathrm{ref}}/1\,\mathrm{s})^2}\right), \tag{9}$$

where $p_{rms,50\mathrm{ms}}$ is the moving RMS over 50 ms. The variations in the amplitude between successive grains is captured as peaks as seen in Fig. 3. For a larger overlap amount the envelop of the synthesized grain is smoother and has a lower peak [Figs. 3(a) and 3(c)]. Similarly, the envelop of the synthesized grain is smoother with a lower peak for the signal

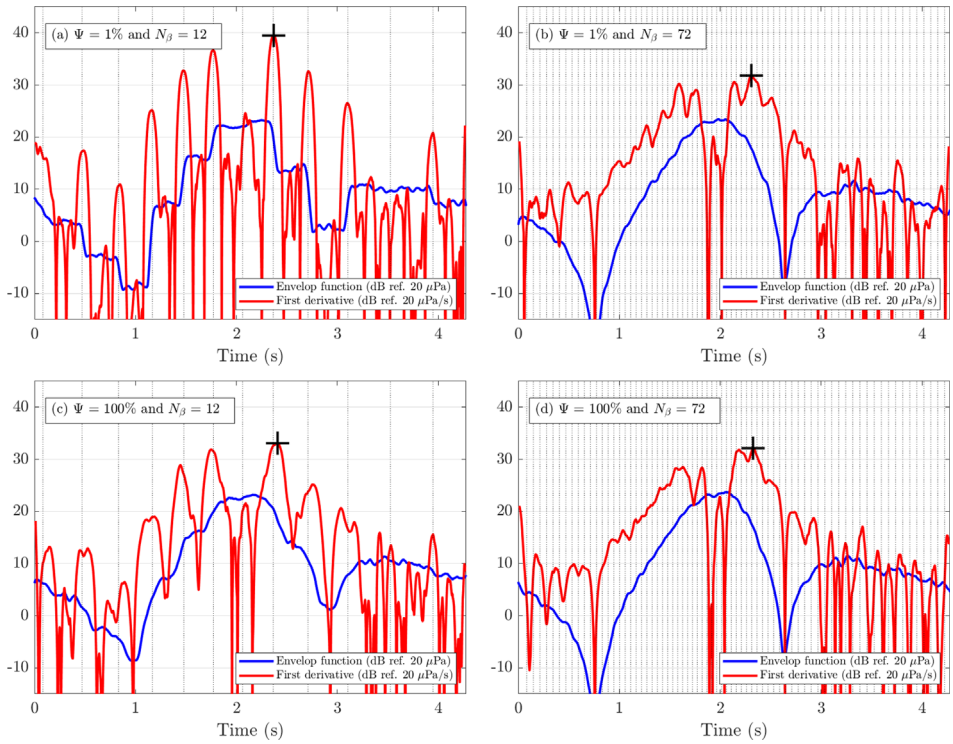

Fig. 3. The SPL of the envelope function (blue) and the SPL of the corresponding time derivative $L_{dp}(t)$ (red). The vertical lines indicate the transitions in time between the grains and the black cross-shows the peak of the derivative.

synthesized with the larger number of discrete angular positions [Figs. 3(a) and 3(b)]. The signal synthesized with a high number of discrete angular positions shows the smoothest envelop function for either extreme values of the overlap amount [Figs. 3(b) and 3(d)]. The maximum rate of change in the amplitude in the synthesized signal, represented as crosses in Fig. 3 is used to quantify the quality of the transitions for different overlap amounts and number of discrete angular positions. The quantified realism of the quality of the transitions for different values of Ψ and N_β is seen in Fig. 4.

From Fig. 4(a) it can be seen that the larger the amount of the overlap between two grains, the smoother is the transition, with the smoothest transition being attained for Ψ = 100%. A difference of approximately 6 dB of the rate of amplitude change is seen between the maximum and minimum values of the overlap. This difference between the change in the amplitudes of each grain for different values of Ψ is clearly audible.[1] As the computational cost is the same for any value of Ψ choosing the optimal amount of Ψ = 100% is beneficial for the synthesis of the signal.

The difference in the amplitude between two adjacent grains changes with the number of discrete angular positions in a single rotation. For a larger number of discrete angular positions, the amplitude change between adjacent grains

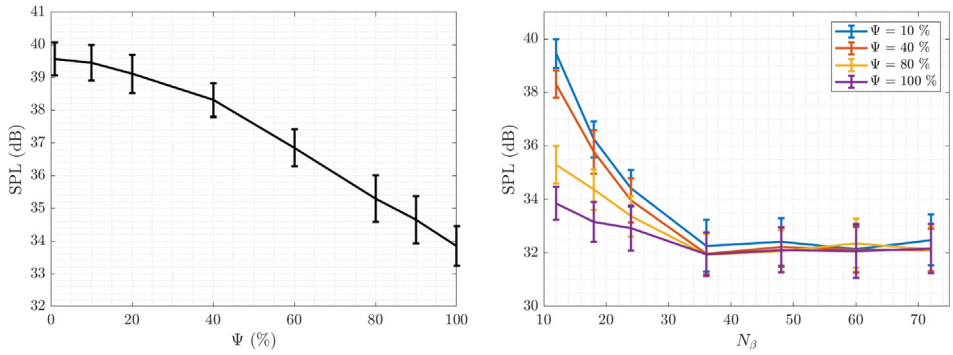

Fig. 4. Maximum of the calculated SPL L_{dp} for (a) different values of Ψ with N_β = 12, (b) different values of N_β with Ψ = 10%, 40%, 80%, and 100%. The error bars show the standard deviation calculated over 50 realizations.

is less, resulting in a smoother transition between grains in the synthesized signal. It is clear from Figs. 3 and 4(b) that the quality of the transitions in the synthesized signal is influenced by the number of discrete angular positions N_β. The quantified quality of the transitions converges for N_β greater than 36. This difference of the quality of the transitions is also audibly distinct,[1] with the largest value of N_β approaching the smoothest signal.

It is apparent that the larger the number of angular positions, the closer the system approaches the continuous rotational motion of the blade. However, the computational time increases proportionally with the number of angular positions N_β. To resolve this particular trade-off between the realism and computational cost, a lower value of N_β can be used with the largest possible value of Ψ. Using $N_\beta = 36$ and $\Psi = 100\%$ the signal can be synthesized approaching the quality that is attained using $N_\beta = 72$ and $\Psi = 10\%$.[1] Note that the synthesis done for this analysis concerns only one single blade segment. Accounting for all the segments of the wind turbine blades induce less noticeable audible artifacts as the transitions of each grain occur at different times due to the propagation delay.

5. Test cases

Using the optimal values of the parameters $\Psi = 100\%$ with $N_\beta = 36$, we synthesize wind turbine trailing edge noise between the frequencies $f_{min} = 100$ Hz and $f_{max} = 6000$ Hz. The synthesis is done for different receiver angular positions τ and constant distance $R = 100$ m from the base of the hub. The hub height is taken as $H = 80$ m. For a wind turbine with rotational speed $\Omega = 1.47$ rad/s, blade span of 45 m divided into eight segments the test cases are done for a constant wind speed of 8 m/s. The contribution of each of the eight segments of the blade is considered to be independent and thus also synthesized separately and finally summed. The resulting synthesized signal from one blade is shifted correspondingly in time to add the response of the second and the third blade of the wind turbine, thus achieving the desired synthesis for the wind turbine noise.

The spectrogram of the synthesized wind turbine trailing edge noise for the receiver at $R = 100$ m and different orientations can be seen in the multimedia files Mm. 1, Mm. 2, and Mm. 3. Strong amplitude modulation is seen in the crosswind position, while there is less variation in the amplitude downwind. The synthesized signals for the other test cases for different observer orientations are available in the supplementary material.[1]

Mm. 1. Video showing the spectrogram of the synthesized sound for the receiver at the downward position ($\tau = 0°$). File type "mp4" (3.4 Mb).

Mm. 2. Video showing the spectrogram of the synthesized sound for the receiver at the inclined position ($\tau = 60°$). File type "mp4" (3.4 Mb).

Mm. 3. Video showing the spectrogram of the synthesized sound for the receiver at the crosswind position ($\tau = 90°$). File type "mp4" (3.4 Mb).

6. Conclusion

The article describes a synthesis tool that converts the frequency-domain model of the wind turbine noise to a time-domain signal. The paper also discusses a cross-fading technique as a component of a window function to account for the relative source-receiver varying distance. A new technique is proposed to objectively estimate the influence of the cross-fading amount and the number of discrete angular positions on the quality of the synthesized signal.

The synthesis that is done is based on Amiet's model for the noise generated by the trailing edge of the wind turbine blades. As this model is physics-based, modification in the parameters such as the receiver position, rotational speed, wind speed, etc., are easily achieved to alter the requirements for the desired synthesized signal. The important parameters that modify the quality of the synthesis are the overlap amount Ψ and the number of grains N_β. From the analysis, we conclude that the optimum value for Ψ is 100% and induce no additional computational cost. We also conclude that the maximum rate of change in the amplitude for different values of N_β converges above $N_\beta = 36$. Considering the computational cost and the noticeable audible difference, $N_\beta = 36$ and $\Psi = 100\%$ provides the optimum values for the synthesis.

To complete the synthesis tool that only accounts for trailing edge noise in this study, other airfoil noise mechanisms such as turbulent inflow noise and stall noise can be added to obtain the corresponding synthesized sound. The synthesis tool does not include the atmospheric propagation effects such as absorption, refraction, and ground reflection. Frequency-domain models such as the parabolic equation can be included in the auralization tool (Barlas *et al.*, 2017; Cotté, 2019). The use of head-related transfer function and binaural rendering with the mono signal generated can be done during the post-processing stage. Other sources of noise such as vegetation and background noise also need to be added to simulate a realistic virtual environment of the required scenario.

Acknowledgments

This project has received funding from the European Union's Horizon 2020 research and innovation program under the Marie Sklodowska-Curie grant agreement No. 812719.

References and links

[1]See supplementary material at https://www.scitation.org/doi/suppl/10.1121/10.0009658 for synthesized sound files with different values of overlap amount Ψ, different number of discrete angular positions N_β, different combination of N_β and Ψ, and synthesized wind turbine trailing edge noise for the receiver at different orientations τ.

Amiet, R. K. (**1976**). "Noise due to turbulent flow past a trailing edge," J. Sound Vib. **47**(3), 387–393.

Arntzen, M., and Simons, D. (**2014**). "Modeling and synthesis of aircraft flyover noise," Appl. Acoust. **84**, 99–106.

Bäckström, T. (**2019**). "Overlap-add windows with maximum energy concentration for speech and audio processing," in *ICASSP 2019-2019 IEEE International Conference on Acoustics, Speech and Signal Processing (ICASSP)*, IEEE, Brighton, UK, pp. 491–495.

Barlas, E., Zhu, W. J., Shen, W. Z., Dag, K. O., and Moriarty, P. (**2017**). "Consistent modelling of wind turbine noise propagation from source to receiver," J. Acoust. Soc. Am. **142**(5), 3297–3310.

Bertagnolio, F., Madsen, H. A., and Fischer, A. (**2017**). "A combined aeroelastic-aeroacoustic model for wind turbine noise: Verification and analysis of field measurements," Wind Energy **20**(8), 1331–1348.

Bolin, K., Nilsson, M. E., and Khan, S. (**2010**). "The potential of natural sounds to mask wind turbine noise," Acta Acust. Acust. **96**(1), 131–137.

Cotté, B. (**2019**). "Extended source models for wind turbine noise propagation," J. Acoust. Soc. Am. **145**(3), 1363–1371.

Fink, M., Holters, M., and Zölzer, U. (**2016**). "Signal-matched power-complementary cross-fading and dry-wet mixing," in *Proceedings of the 19th International Conference on Digital Audio Effects (DAFx-16)*.

Georgiou, F., Hornikx, M., and Kohlrausch, A. (**2019**). "Auralization of a car pass-by using impulse responses computed with a wave-based method," Acta Acust. Acust. **105**(2), 381–391.

Goody, M. (**2004**). "Empirical spectral model of surface pressure fluctuations," AIAA J. **42**(9), 1788–1794.

Hansen, K. L., Nguyen, P., Micic, G., Lechat, B., Catcheside, P., and Zajamšek, B. (**2021**). "Amplitude modulated wind farm noise relationship with annoyance: A year-long field study," J. Acoust. Soc. Am. **150**(2), 1198–1208.

IEC (**2012**). 61400-11: 2012, *Wind Turbines–Part 11: Acoustic Noise Measurement Techniques* (International Electrotechnical Commission, Geneva, Switzerland).

Jagla, J., Maillard, J., and Martin, N. (**2012**). "Sample-based engine noise synthesis using an enhanced pitch-synchronous overlap-and-add method," J. Acoust. Soc. Am. **132**(5), 3098–3108.

Langford, S. (**2013**). *Digital Audio Editing: correcting and Enhancing Audio in Pro Tools, Logic Pro, Cubase, and Studio One* (CRC Press, Boca Raton, FL).

Lee, S., Lee, S., and Lee, S. (**2013**). "Numerical modeling of wind turbine aerodynamic noise in the time domain," J. Acoust. Soc. Am. **133**(2), EL94–EL100.

Oerlemans, S., and Schepers, J. G. (**2009**). "Prediction of wind turbine noise and validation against experiment," Int. J. Aeroacoust. **8**(6), 555–584.

Pedersen, E., and Persson Waye, K. (**2004**). "Perception and annoyance due to wind turbine noise—A dose–response relationship," J. Acoust. Soc. Am. **116**(6), 3460–3470.

Pieren, R., Heutschi, K., Müller, M., Manyoky, M., and Eggenschwiler, K. (**2014**). "Auralization of wind turbine noise: Emission synthesis," Acta Acust. Acust. **100**(1), 25–33.

Pieren, R., Heutschi, K., Wunderli, J. M., Snellen, M., and Simons, D. G. (**2017**). "Auralization of railway noise: Emission synthesis of rolling and impact noise," Appl. Acoust. **127**, 34–45.

Roger, M., and Moreau, S. (**2010**). "Extensions and limitations of analytical airfoil broadband noise models," Int. J. Aeroacoust. **9**(3), 273–305.

Rozenberg, Y., Robert, G., and Moreau, S. (**2012**). "Wall-pressure spectral model including the adverse pressure gradient effects," AIAA J. **50**(10), 2168–2179.

Sinayoko, S., Kingan, M., and Agarwal, A. (**2013**). "Trailing edge noise theory for rotating blades in uniform flow," Proc. R. Soc. A: Math. Phys. Eng. Sci. **469**(2157), 20130065.

Tian, Y., and Cotté, B. (**2016**). "Wind turbine noise modeling based on Amiet's theory: Effects of wind shear and atmospheric turbulence," Acta Acust. Acust. **102**(4), 626–639.

Van den Berg, G. (**2006**). "Wind-induced noise in a screened microphone," J. Acoust. Soc. Am. **119**(2), 824–833.